Cluster glass properties and magnetic phase separation studies of $Nd_xBi_{0.5-x}Sr_{0.5}MnO_3$ (x = 0.1, 0.2, 0.3 and 0.4)

2009 J. Phys.: Condens. Matter 21 195409

(http://iopscience.iop.org/0953-8984/21/19/195409)

J. Phys.: Condens. Matter **21** (2009) 195409 (7pp) doi:10.1088/0953-8984/21/19/195409

Cluster glass properties and magnetic phase separation studies of $Nd_xBi_{0.5-x}Sr_{0.5}MnO_3$ ($x = 0.1$, 0.2, 0.3 and 0.4)

S Savitha Pillai[1], P N Santhosh[1], N Harish Kumar[1], P John Thomas[2] and F Tuna[2]

[1] Department of Physics, Indian Institute of Technology, Madras, Tamil Nadu 600036, India
[2] School of Chemistry, University of Manchester, Oxford Road, Manchester M13 9PL, UK

E-mail: santhosh@physics.iitm.ac.in

Received 7 August 2008, in final form 28 March 2009
Published 22 April 2009
Online at stacks.iop.org/JPhysCM/21/195409

Abstract

The crystal structure, dc and ac magnetic susceptibility, electron spin resonance and magnetoresistive behavior of $Nd_xBi_{0.5-x}Sr_{0.5}MnO_3$ ($x = 0.1$, 0.2, 0.3 and 0.4) compounds are studied. The Rietveld analysis of the XRD data shows that the samples crystallize in an orthorhombic perovskite structure, with $Pbnm$ space group for $x = 0.1$ and 0.2 and $Imma$ space group for $x = 0.4$ and 0.3. Magnetic studies reveal that substituting Bi with Nd collapses the robust charge ordered AFM state of $Bi_{0.5}Sr_{0.5}MnO_3$ to an inhomogeneous magnetic state. As Nd concentration increases there is a gradual appearance of cluster glass behavior. ESR studies reveal that the NBSMO system phase separates into ferromagnetic and antiferromagnetic regions below the transition temperature.

(Some figures in this article are in colour only in the electronic version)

1. Introduction

Recently, bismuth-based manganites $Bi_xA_{1-x}MnO_3$ (A = Ca, Sr, etc) have attracted considerable attention due to their high temperature charge/orbital ordering phenomena [1–5]. In contrast with rare-earth-based manganites, bismuth-based manganites have not been extensively studied due to the lack of an appreciable magnetoresistive property [3]. In bismuth-based manganites the charge ordering (CO) occurs at a temperature which is well above the room temperature and these compounds do not follow the one-electron bandwidth tuning model used to quantitatively explain the T_{CO} (charge ordering temperature) variation [1, 3]. For example, the CO state in $Bi_{0.5}Sr_{05}MnO_3$ (BSMO) occurs at 475 K and this state is stable even with an applied magnetic field of 40 T [4]. This unique electronic state is manifested by the presence of a Bi^{3+} lone pair with strong $6s^2$ character. The orientation of the $6s^2$ lone pair towards a surrounding anion can produce a local distortion or even hybridization between Bi 6s orbits and O 2p orbits. This reduces the movement of e_g electrons through the Mn–O–Mn bonds and strongly favors charge localization [4, 5]. Recent studies on doped manganites revealed that the nanoscale phase separation due to competition between the ferromagnetic phase (FM) and charge ordered antiferromagnetic phase yield the CMR (colossal magnetoresistance) phenomenon [7, 8]. In the case of rare-earth-based manganites the stability of these competing phases can be controlled by the effective one-electron bandwidth of the e_g orbital and the variance of the A-site ionic radii [9]. $Nd_{0.5}Sr_{0.5}MnO_3$ (NSMO) undergoes a ferromagnetic transition (FM) at 250 K followed by a charge ordered CE-type antiferromagnetic transition around 160 K [6]. Here we have investigated the solid solution, $Nd_xBi_{0.5-x}Sr_{0.5}MnO_3$ of the above two systems, BSMO and NSMO. The study of this solid solution is of importance in the context of the search for the colossal magnetoresistive properties in bismuth manganites and their anomalous structural and magnetic behavior compared with bismuth-or rare-earth-based manganites [10].

Table 1. Structural parameters of $Nd_xBi_{0.5-x}Sr_{0.5}MnO_3$ ($x = 0.1$, 0.2, 0.3 and 0.4).

NBSMO	$x = 0.1$	$x = 0.2$	$x = 0.3$	$x = 0.4$
Space group	*Pbnm*	*Pbnm*	*Imma*	*Imma*
a (Å)	5.5238(8)	5.5061(4)	5.4726(4)	5.4441(3)
b (Å)	5.5327(8)	5.5364(3)	7.6318(6)	7.6365(4)
c (Å)	7.6161(4)	7.6243(5)	5.5107(4)	5.4765(3)
V (Å^3)	232.760(3)	232.414(4)	230.158(9)	227.680(2)
Nd/Bi/Sr x	0.0028(5)	−0.0024(8)	0	0
Nd/Bi/Sr y	0.0005(5)	−0.0047(8)	0.25	0.25
Nd/Bi/Sr z	0.25	0.25	−0.0059(7)	−0.0101(5)
Mn x	0.5	0.5	0	0
Mn y	0	0	0	0
Mn z	0	0	0.5	0.5
O_1 x	−0.058(6)	−0.064(6)	0	0
O_1 y	0.552(6)	0.568(5)	0.25	0.25
O_1 z	0.25	0.25	0.425(2)	0.4335
O_2 x	−0.275(9)	−0.268(5)	0.75	0.75
O_2 y	0.236(8)	0.229(6)	−0.031(2)	−0.024(9)
O_2 z	−0.029(2)	−0.034(2)	0.25	0.25
Bi–O (Å)	2.601(1)	2.628(4)	2.649(4)	2.654(5)
Mn–O (Å)	1.963(4)	1.961(1)	1.954(1)	1.945(2)
Mn–O–Mn (deg)	160.55(2)	160.75(3)	160.85(3)	163.80(2)
$R_{wp\%}$	6.9	6.98	6.05	5.38
$R_{P\%}$	5.21	5.40	4.59	4.25
$\langle r_A \rangle$ (Å)	1.1003	1.0958	1.0909	1.0862

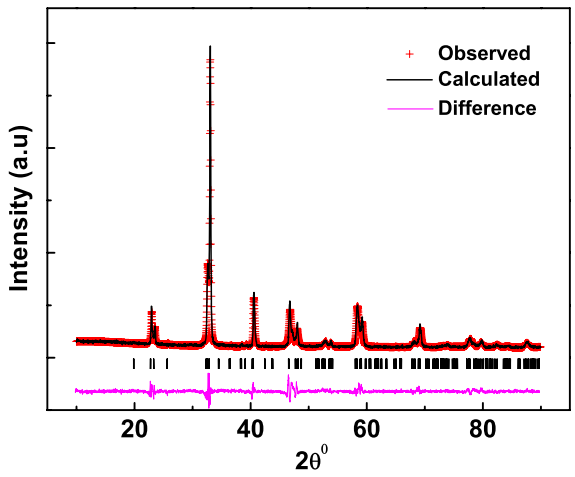

Figure 1. Rietveld refinement profiles of x-ray powder diffraction data for $Nd_xBi_{0.5-x}Sr_{0.5}MnO_3$ ($x = 0.1$). The solid line is the calculated profile and a difference curve is plotted at the bottom.

2. Experimental details

Polycrystalline samples of $Nd_xBi_{0.5-x}Sr_{0.5}MnO_3$ ($x = 0.1$, 0.2, 0.3 and 0.4) were prepared by the solid state method using stoichiometric mixtures of high purity Bi_2O_3, $SrCO_3$, Nd_2O_3 and MnO_2. The mixtures were heated in alumina crucibles in air at temperatures ranging from 900 to 1200 °C for 24 h duration (in 100 °C increments) with intermediate grinding. The heating process was continued until the materials were determined to be of a single phase by x-ray powder diffraction. Powder XRD patterns of the samples were recorded using a PANalytical X'pertPro diffractometer with step size of 0.004, using Cu Kα radiation. Resistivity measurements were performed using the conventional four-probe method in the temperature range 4–300 K. Resistance in the presence of a magnetic field (up to 11 T) was measured down to liquid helium temperatures using a Janis 12 T magnet cryostat. DC magnetization data was measured using a SQUID magnetometer. A home-made ac susceptometer was employed for the measurements of ac magnetic susceptibility in the temperature range 78–300 K. The amplitude of the ac field in these experiments was 15 Oe. The ESR spectra were recorded with a Varian E-112 continuous wave spectrometer at X-band frequency (≈9.35 GHz) and approximately 0.03 g of fine powder was used for the measurement.

3. Results and discussion

3.1. Structural properties

The Rietveld analysis of the XRD data shows that the samples were all single phase with an orthorhombic perovskite structure. The Rietveld refinements were carried out by using structural parameters of end members BSMO (*Pbnm*) or NSMO (*Imma*) as starting values [11, 12]. It was found that NBSMO with compositions $x = 0.1$ and 0.2 crystallizes with *Pbnm* space group whereas the other two compositions, $x = 0.3$ and 0.4, crystallize with *Imma* space group. The results from Rietveld refinement of XRD patterns of $x = 0.1$ is shown in figure 1. The refined structural parameters are given in table 1. The change from *Pbnm* to *Imma* space group reveals the finite structural changes associated with the octahedral tilt with increasing Nd doping. The value of $b/\sqrt{2}$ is less than a or c, suggesting that the combination of a co-operative Jahn–Teller distortion (orbital ordering) and octahedral tilting produces the O'-type lattice distortion in samples [13]. The presence of a lone pair of Bi^{3+} ions

enhances the hybridization between 6s orbitals of Bi^{3+} and 2p orbitals of O^{2-} orbitals that leads to a covalent character of the Bi–O bonds as well as a change in Bi–O bond lengths. When the $6s^2$ character is dominant, the value of the ionic radius of Bi^{3+} (1.16 Å) increased to 1.24 Å and the average radius of the A-site cation is not a significant factor in tuning the structural properties [1, 3, 14, 15]. However, the cell volume, Mn–O bond lengths and Mn–O–Mn bond angle vary in accordance with Nd doping concentration, consistent with the fact that structural changes occur in accordance with the average radius of A-site cations, $\langle r_A \rangle$ of the NBSMO system. Unlike La-based bismuth systems, the screening of a highly polarizable $6s^2$ lone pair of Bi^{3+} in the lattice variations is assigned to the large ionic size difference between the Nd/Bi combination compared to La and Bi ions [3, 14].

3.2. Magnetic properties

Figure 2 shows the temperature dependence of the zero-field-cooled (ZFC) and field-cooled (FC) dc magnetization of the NBSMO system at a field of 100 Oe. The ferromagnetic transition temperatures, T_Cs, obtained from a minimum value of temperature in the dM/dT versus T curve are 272 K, 274 K, 275 K and 276 K for $x = 0.1$, 0.2, 0.3 and 0.4, respectively. The large thermal irreversibility in ZFC and FC magnetizations indicate the absence of true long range magnetic order in this system [16–20]. The ZFC magnetic moments of all samples were found to decrease below 200 K. The ZFC magnetization curve of the compositions $x = 0.3$ and 0.4 exhibits a clear cusp-like behavior just below the ferromagnetic transition temperatures and, for the other compositions $x = 0.1$ and 0.2, the cusp becomes broader. The splitting of ZFC and FC magnetizations and the cusp-like behavior in the ZFC magnetization are the hallmarks for spin glass/cluster glass systems or the coexistence of antiferromagnetic domains with ferromagnetic domains [18–20].

To probe the glassy magnetic behavior, the frequency-dependent ac susceptibility (χ_{ac}) measurements of the samples were performed. In glassy compounds, the ac susceptibility shows a frequency (f)-dependent cusp at an effective spin freezing temperature T_f. Figures 3(a)–(d) show the temperature dependence of the ac susceptibility of the NBSMO samples with different frequencies ranging from 133 to 1333 Hz. The χ_{ac} of $x = 0.1$ and 0.2 samples do not have a pronounced peak below the ferromagnetic transition at any frequencies. However, in the case of $x = 0.3$ and 0.4 samples, the χ_{ac} exhibits a maximum around 200 K, which coincides with the ZFC magnetization cusp temperature. The peak temperature, T_f of χ_{ac} is found to be frequency-dependent and shifts to lower temperature with decreasing frequency and is found to satisfy the critical slowing-down model [18, 21]. In this model the relaxation time, τ is related to the reduced temperature, $\varepsilon = [T_f - T_g]/T_g$ as $\tau/\tau_0 = \varepsilon^{-z\nu}$, where τ_0 is the microscopic flipping time of the fluctuating entities, ν and z are critical exponents and T_g is the true spin glass temperature, determined by extrapolating the T_f–f curve to zero frequency. The relaxation time corresponds to the measured frequency in terms of $\tau = 1/2\pi f$. The insets of figures 3(c) and (d) show the

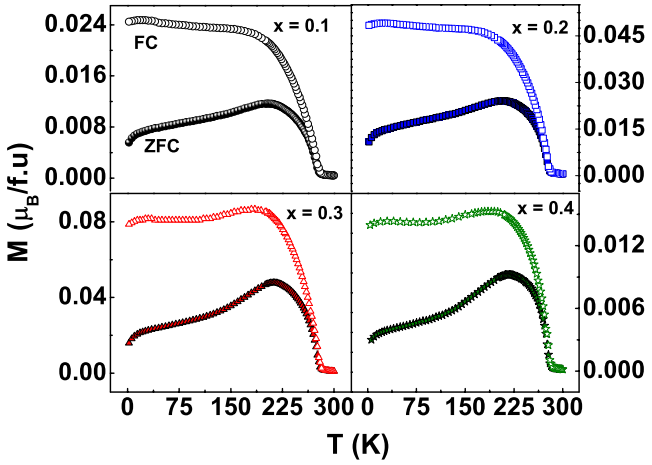

Figure 2. ZFC (open characters) and FC (full characters) magnetization of $Nd_xBi_{0.5-x}Sr_{0.5}MnO_3$ ($x = 0.1$, 0.2, 0.3 and 0.4).

dynamical scaling of τ with reduced temperature, ε. The obtained values of τ_0 for the compositions $x = 0.3$ and $x = 0.4$ are 4.6×10^{-6} s and 3.6×10^{-6} s, respectively. The value of the product $z\nu$ is 1.06 for $x = 0.3$ and 1.03 for $x = 0.4$. The value of τ_0 of the present system ($\sim 10^{-6}$) is much longer than for the conventional spin glass ($\sim 10^{-13}$ s), which indicates the presence of magnetic clusters with weak intercluster interactions, i.e. the cluster glass state [18, 22, 23]. The frequency shift of the peak position $C = \frac{\Delta T_f}{T_f \Delta \log f}$ is found to be 0.034 for the sample $x = 0.3$ and is 0.049 for the sample $x = 0.4$. These values are found to be higher than the conventional spin glasses (homogeneous freezing) and suggest the presence of inhomogeneous cluster freezing (weak interactions) of the present system [18]. Moreover, the large difference between ZFC and FC magnetizations, the continuous increase of FC magnetization below T_C and the occurrence of irreversibility just above T_C also support the cluster glass state in these compounds [23, 24]. In the case of typical spin glasses, the irreversibility starts below the freezing temperature, T_f, the FC magnetization remains constant below the freezing temperature and the drop in ZFC magnetization occurs at low temperature [22].

The combined results of dc and ac magnetizations suggest that there is an absence of typical glassy nature in $x = 0.1$ and 0.2 samples. However, the large difference in ZFC and FC magnetizations and the drop in ZFC magnetization at low temperatures are not signatures of a true ferromagnetic state. The intra-cluster interactions would result in a decrease of the ZFC magnetic moment and the ferromagnetic state of these compositions [22]. Similar to other glassy compounds, the A-site cation doping concentration also has a significant effect on the present system. The change in the doping concentration varies the competition between the ferromagnetic and antiferromagnetic interactions along with the randomness in cation distribution, which in turn results in the growth of short range clusters. The cluster glass state appears when the ferromagnetic clusters exceed the charge ordered AFM interactions [22, 23]. In NBSMO systems, the number of ferromagnetic clusters increases with increasing Nd

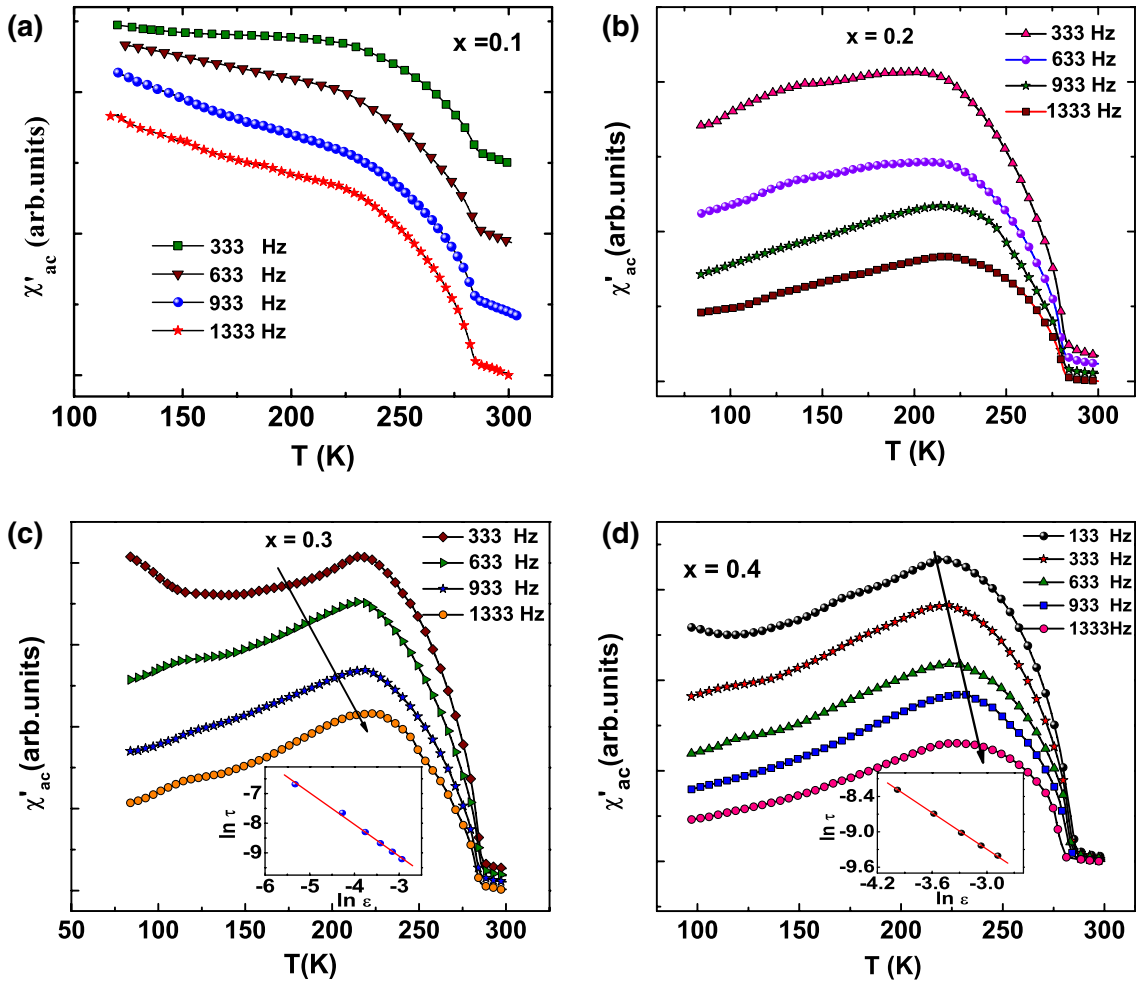

Figure 3. ((a)–(d)): temperature dependence of ac susceptibility at several ac frequencies of $Nd_xBi_{0.5-x}Sr_{0.5}MnO_3$ with (a) $x = 0.1$, (b) $x = 0.2$, (c) $x = 0.3$ and (d) $x = 0.4$. Inset ((c) and (d)): dynamical scaling of τ with reduced temperature, ε of NBSMO with $x = 0.3$ and 0.4. Symbols represent the data points while the line is the linear fit.

content, which enhances the random freezing of spins (cluster glass) near the transition temperature, T_C.

The magnetization versus field, H (up to 8 T), of the sample $x = 0.1$ at temperatures well below T_C and above T_C are shown in figure 4. The isotherm above T_C follows the characteristic of a normal paramagnetic state. However, the behavior of the isotherm well below T_C differs from the typical ferromagnetic behavior and there is no sign of saturation even with a field of 8 T. The magnetic moment value at 8 T is found to be ≈0.4 μ_B/f.u., which is much lower than the expected magnetic moment value (≈3.5 μ_B/f.u.) for ferromagnetic Mn^{3+}/Mn^{4+} combinations [24]. The absence of saturation indicates the coexisting of an AFM phase with FM phase in the sample [25].

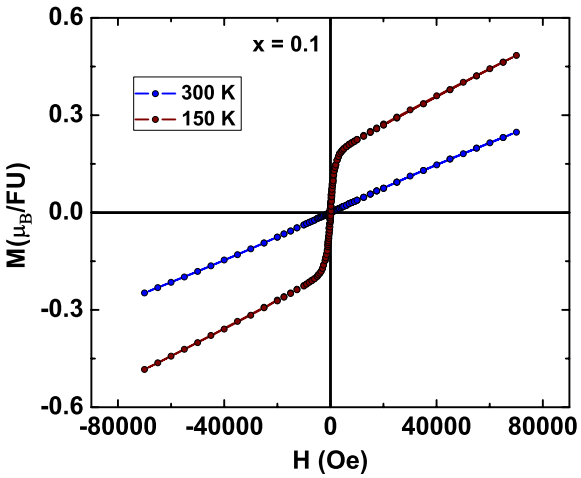

Figure 4. Magnetic hysteresis curve for $Nd_{0.1}Bi_{0.4}Sr_{0.5}MnO_3$ at 300 and 150 K.

3.3. Electron spin resonance studies (ESR)

Electron spin resonance measurements of the samples were carried out to study the magnetic state of the system at different temperatures and the data was collected in the temperature range from 400 to 130 K. Figure 5 shows the ESR spectra of NBSMO with $x = 0.2$. The ESR spectra in the paramagnetic region consist of a single line with a Lorentzian shape and in the vicinity of the transition temperature T_C the line gradually broadens. Below T_C, the resonance shifts to lower fields and broad spectra are fitted into two Lorentzians. The ESR spectra were fitted by a differential Lorentzian lineshape of the form

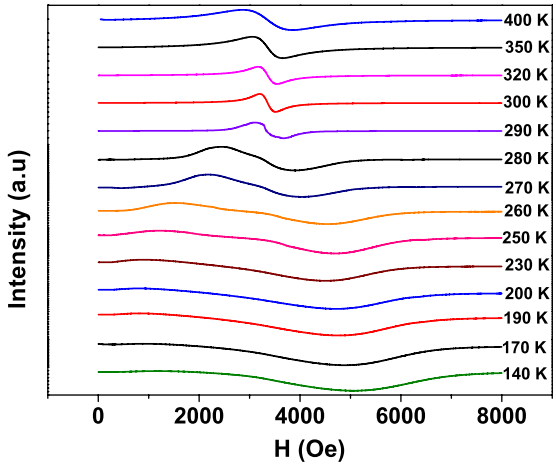

Figure 5. ESR spectra of $Nd_{0.2}Bi_{0.3}Sr_{0.5}MnO_3$ at various temperatures.

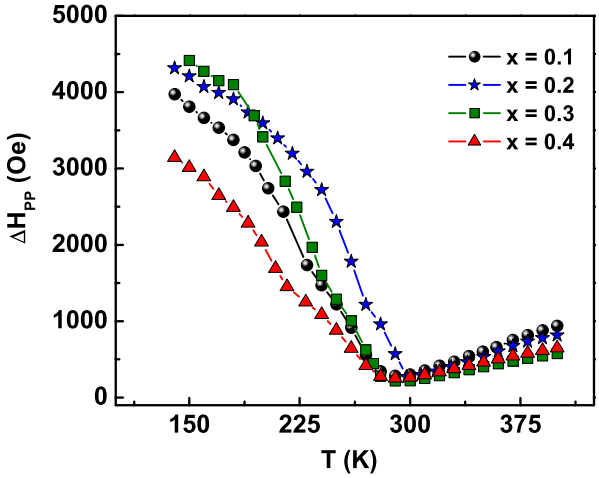

Figure 6. Temperature variation of peak-to-peak ESR linewidth (ΔH_{PP}) of the samples.

$\frac{dP}{dH} = \frac{d}{dH}[\frac{\Delta H}{(H-H_0)^2+\Delta H^2}]$, where P is the power absorbed by the sample from the transverse magnetic microwave field and keeping the resonance field H_0, the linewidth ΔH and the intensity of each line as adjustable parameters.

The temperature dependence of the peak-to-peak linewidth $\Delta H_{PP} = \sqrt{3}/2(\Delta H)$ is shown in figure 6. The linewidth decreases linearly with the decrease of temperature in the PM regime and goes through a minimum value near the ordering temperature ($T_{min} \approx T_C$) and below T_C a fast broadening of the linewidth is observed in all samples. The temperature-dependent narrowed linewidth in manganites is due to the presence of the strong electron–phonon coupling arising from both anisotropic interactions and Dzyaloshinsky–Moriya (DM) interactions. The crystal field effect and Jahn–Teller distortion cause the anisotropic interactions while antisymmetric exchange terms arise from DM interaction, $Dij(Si * Sj)$ leading to strong spin–lattice interactions. DM interactions result in phonon modulation, which cause spin flipping and thereby changes in the exchange energy [26, 27]. The slope of the linear temperature dependence of ΔH_{PP} in the PM regime is found to be decreasing with increasing x value. This indicates the decreasing of the strength of the spin–lattice interaction with increase in Nd content [28]. The linewidth minima are obtained at temperatures ~285 K for $x = 0.1$, 0.3 and 0.4 and ~300 K for $x = 0.2$. The linewidth minimum has been observed in various rare-earth-doped manganites at temperatures well above the corresponding Curie temperature, indicating the presence of FM spin clusters in the PM regime, i.e. $T_{min} \approx 1.1T_C$. The absence of additional resonance spectra above T_C and a linewidth minimum at $T_{min} \approx T_C$ indicates the absence of FM spin clusters in the PM region [29, 30]. The minimum near the transition is attributed to weak spin correlations due to magnetic phase transitions, which is significant for magnetically inhomogeneous samples [30]. Broadening of the linewidth below the transition temperature is due to the demagnetizing field arising from the non-magnetic inclusions such as pores between grains, the change in the spin–lattice interactions arising from the ordering of magnetic moments and heterospin interactions due to the real space ordering of Mn^{3+} and

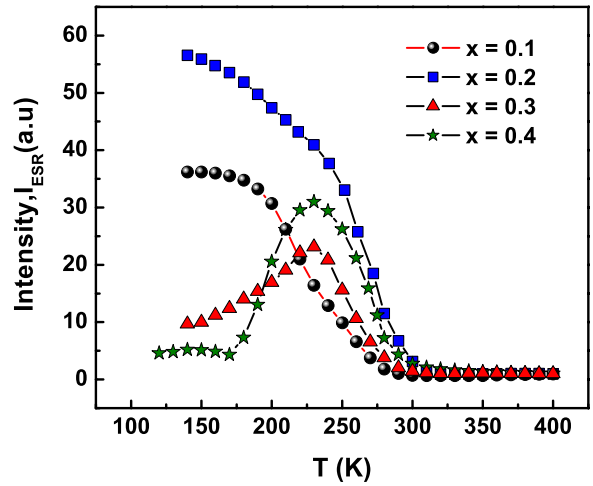

Figure 7. Temperature variation of double integrated ESR intensity of the samples.

Mn^{4+} ions [31]. The temperature dependence of the linewidth provides evidence for magnetic transitions in the vicinity of T_C.

The temperature dependence of the ESR integrated intensity, I, is shown in figure 7. The intensity of the resonance signal is found to drastically vary with Nd doping. As the temperature reduces, the intensity of the compositions $x = 0.3$ and 0.4 reaches a maximum value at about 230 K, and below this temperature the intensity is found to decrease. The ESR intensity is proportional to the corresponding magnetic phase. The drop of the ESR intensity can be due to the appearance of non-resonant microwave absorption [32], the loss of the ESR signal in the antiferromagnetic phase [33] or the appearance of the glass-like state caused by some magnetic moments freezing at high frequency [34]. If we consider the correlation between ESR intensity with ac and dc magnetizations, the glassy state seems to be responsible for the drop in intensity. The temperature dependence of the ESR intensity confirms the existence of a glassy state of $x = 0.3$ and 0.4 samples. In the case of $x = 0.1$ and 0.2 samples, the temperature dependence

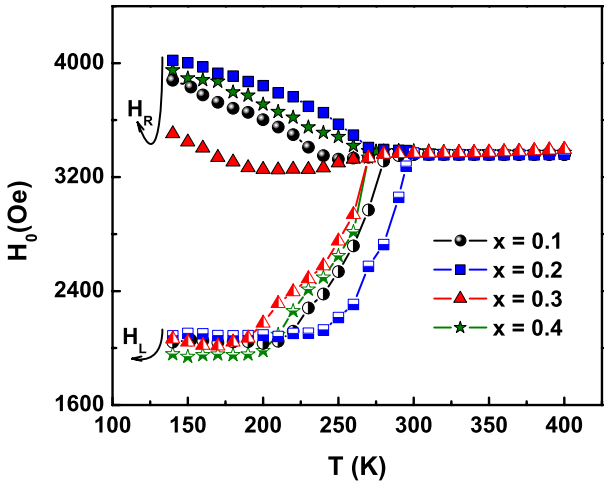

Figure 8. Temperature variation of resonance field (H_0) of the samples.

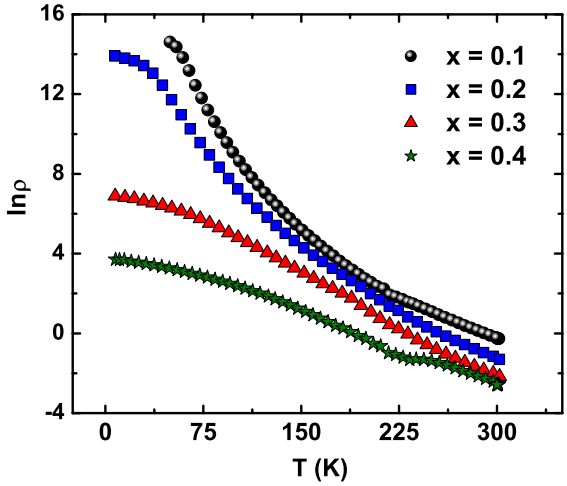

Figure 9. The temperature-dependent resistivity of $Nd_xBi_{0.5-x}Sr_{0.5}MnO_3$ ($x = 0.1$, 0.2, 0.3 and 0.4).

of ESR intensity rises sharply in the vicinity of the transition temperature and continues to increase below T_C.

The temperature-dependent ESR resonant fields (figure 8) clearly show the coexistence of different magnetic phases in the NBSMO system. As mentioned above, the ESR spectra could be fitted by two Lorentzian functions below T_C. The lower (H_L) and higher field (H_H) resonances are attributed to ferromagnetic and antiferromagnetic coupling between the Mn ions, respectively [31, 35]. The increase of magnetization due to the FM alignment of Mn spin moments drives an increase in the internal magnetic field. Hence, FM resonance shifts to lower field and AFM resonance occurs at higher field. In the vicinity of T_C, the FM phase coexists with a paramagnetic phase and below T_C one of the phases changes to an AFM phase for all the compositions. However, for the sample $x = 0.1$, the PM state exists well below T_C and this paramagnetic state changes to an antiferromagnetic state at 230 K. The ac and dc magnetic susceptibility studies do not show any signature of the superparamagnetic behavior in this sample, which may be due to the predominant FM character [18]. The origin of the phase separation or the magnetic inhomogeneity is ascribed to the competition between the charge ordered AFM and FM interactions arising from the A-site cation disorder or randomness.

3.4. Magneto-transport properties

Figure 9 shows the temperature-dependent resistivity of NBSMO samples. All samples show an insulating behavior and the conductivity increases with increasing Nd content. This is due to the delocalization of charge carriers with Nd doping, which enhances the spatial overlap between Mn e_g and O 2p orbitals and thereby increases the mobility of carriers [9, 13]. Field-dependent magnetoresistance (MR) at 300 and 100 K of all samples are shown in figures 10(a) and (b). Negative MR of 14, 24 and 27% observed at 300 K for an applied field of 11 T for the composition $x = 0.2$, 0.3 and 0.4, respectively. No appreciable MR is observed in the $x = 0.1$ compound at 300 K. Below the transition temperature all the compounds show high values of MR and it increases with increase of the Nd content. The NBSMO with $x = 0.4$ shows a negative MR of 88% at 100 K under an applied field of 11 T. The temperature-dependent MR of $x = 0.3$ in a magnetic field of 11 T is also shown in the inset of figure 10(a). The negative MR increases with decreasing temperature and shows a maximum of 95% at 27 K. It has been reported that the end member BSMO does not have significant MR even at very high field (8 T) [3]. In the BSMO system, the partial hybridization of the Bi $6s^2$ electrons with some O 2p orbitals leads to a reduction of the charge transfer of bonding e_g electrons from Mn^{3+} to Mn^{4+} ions which results in the robust charge ordering. However, our results indicate that a small doping of Nd enhances the MR properties of BSMO. Doping with Nd ions causes local inhomogeneity that induces randomness in potential energy, transfer energy and exchange interaction and favors magnetoresistive properties [7, 9]. The field-dependent MR at 100 K of all samples exhibits prominent hysteresis, which arises from the slow relaxation of the remnant field due to the coexistence of different magnetic states [36].

4. Summary

In summary, we have studied structural, magnetic, ESR and magneto-transport properties of Nd-doped $Bi_{0.5}Sr_{0.5}MnO_3$. The magnetic measurements reveal that Nd doping collapses the robust charge ordered AFM state of BSMO and leads to an inhomogeneous magnetic state. The compounds with large Nd content exhibit typical cluster glass features. Magneto-transport studies indicate that the significant role of the $6s^2$ lone pair of Bi^{3+} ions is suppressed by Nd doping. The structural studies reveal that the lattice variations occur in accordance with change in the average radius of A-site cations, which is in contrast to the La-doped Bi–Sr–Mn–O systems [3]. The observed magnetic and transport properties reveal that the change in Nd concentration varies the strength of ferromagnetic and antiferromagnetic interactions along with the randomness leading to phase separation behavior. Coexisting clusters of competing phases result in the CMR

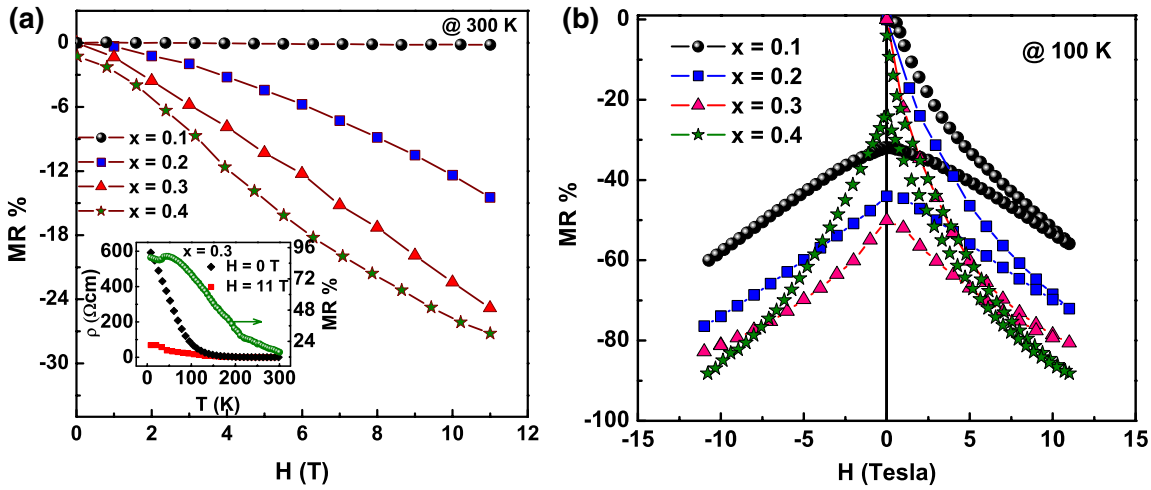

Figure 10. The field dependence of MR at (a) 300 K and (b) 100 K of all samples. Inset (a): temperature dependence of MR at 11 T of $Nd_{0.3}Bi_{0.2}Sr_{0.5}MnO_3$.

properties of the NBSMO system in tune with the current theoretical model of Sen *et al* [7].

Acknowledgments

PNS thanks the Department of Science and Technology (DST), India for research funding. SSP thanks the Council for Scientific and Industrial Research, India for a Senior Research Fellowship. The authors would like to thank the low temperature high magnetic field measurement facility at IISc Bangalore for help in MR measurements.

References

[1] Garcia-Munoz J L, Frontera C, Aranda M A G, Llobet A and Ritter C 2001 *Phys. Rev.* B **63** 064415
[2] Santhosh P N, Goldberger J, Woodward P M, Vogt T, Lee W P and Epstein A J 2000 *Phys. Rev.* B **62** 14928
[3] Frontera C, Garcia-Munoz J L, Llobet A, Aranda M A G, Ritter C, Respaud M and Vanacken J 2001 *J. Phys.: Condens. Matter* **13** 1071
[4] Garcia-Munoz J L, Frontera C, Respaud M, Giot M, Ritter C and Capdevila X G 2005 *Phys. Rev.* B **72** 054432
[5] Hervieu M, Maignan A, Martin C, Nguyen N and Raveau B 2001 *Chem. Mater.* **13** 1356
[6] Tokura Y and Nagaosa N 2000 *Science* **288** 462
[7] Sen C, Alvarez G and Dagotto E 2007 *Phys. Rev. Lett.* **98** 127202
[8] Tokura Y 2006 *Rep. Prog. Phys.* **69** 797
[9] Yu X Z, Arima T, Kaneko Y, He J P, Mathieu R, Asaka T, Hara T, Kimoto K, Matsui Y and Tokura Y 2007 *J. Phys.: Condens. Matter* **19** 172203
[10] Savitha Pillai S, Santhosh P N, Markandeyulu G, John Thomas P and Tuna F 2008 *J. Appl. Phys.* **103** 07F721
[11] Frontera C, Garcia-Munoz J L, Aranda M A G, Ritter C, Llobet A, Respaud M and Vanacken J 2001 *Phys. Rev.* B **64** 054401
[12] Woodward P M, Vogt T, Cox D E, Arulraj A, Rao C N R, Karen P and Cheetham A K 1998 *Chem. Mater.* **10** 3652
[13] Woodward P M, Vogt T, Cox D E, Rao C N R and Cheetham A K 1999 *Chem. Mater.* **11** 3528
[14] Kirste A, Goiran M, Respaud M, Vanaken J, Broto J M, Rakoto H, Von Ortenberg M, Frontera C and Garcia-Munoz J L 2003 *Phys. Rev.* B **67** 134413
[15] Garcia-Munoz J L, Frontera C, Aranda M A G, Ritter C, Llobet A, Respaud M, Goiran M, Rakoto H, Masson O, Vanacken J and Broto J M 2003 *J. Solid State Chem.* **171** 84
[16] Ryzhov V A, Lazuta A V, Smirnov O P, Kiselev I A, Chernenkov Y P, Borisov S A, Troaynchuk I O and Khalyavin D D 2005 *Phys. Rev.* B **72** 134427
[17] Lobanov M V, Balagurov A M, Pomjakushin V J, Fischer P, Gutmann M, Abakumov A M, Dyachenko O G, Antipov E V, Lebedev O I and Van Tendeloo G 2000 *Phys. Rev.* B **61** 8941
[18] Mydosh J A 1993 *Spin Glasses* (London: Taylor and Francis)
[19] Wang K F, Wang Y, Wang L F, Dong S, Li D, Zhang Z D, Yu H, Li Q C and Liu J M 2006 *Phys. Rev.* B **73** 134411
[20] Savitha Pillai S, Rangarajan G, Raju N P, Epstein J and Santhosh P N 2007 *J. Phys.: Condens. Matter* **19** 496221
[21] Mathieu R, Akahoshi D, Asamitsu A, Tomioka Y and Tokura Y 2004 *Phys. Rev. Lett.* **93** 227202
[22] Freitas R S, Ghivelder L, Damay F, Dias F and Cohen L F 2001 *Phys. Rev.* B **64** 144404
[23] Mukherjee S, Ranganathan R, Anilkumar P S and Joy P A 1996 *Phys. Rev.* B **54** 9267
[24] Maignan A, Martin C, Damay F, Raveau B and Hejtmanek J 1998 *Phys. Rev.* B **58** 2758
[25] Karmakar S, Taran S, Chaudhuri B K, Sakata H, Sun C P, Huang C L and Yang H D 2006 *Phys. Rev.* B **74** 104407
[26] Seehra M S, Ibrahim M M, Suresh Babu V and Srinivasan G 1996 *J. Phys.: Condens. Matter* **8** 11283
[27] Cooper B R and Keffer F 1962 *Phys. Rev.* **125** 896
[28] Ulyanov A N, Yu S C, Min S G and Levchenko G G 2002 *J. Appl. Phys.* **91** 7926
[29] Oseroff S B, Torikachvili M, Singley J, Ali S, Cheong S W and Schultz S 1996 *Phys. Rev.* B **53** 6521
[30] Causa M T, Tovar M, Caneiro A, Prado F, Ibanez G, Ramos C A, Butera A, Alascio B, Obradors X, Pinol S, Rivadulla F, Vazquez-Vazquez C, Lopez-Quintela M A, Rivas J, Tokura Y and Oseroff S B 1998 *Phys. Rev.* B **58** 3233
[31] Autret C, Gervais M, Gervais F, Raimboux N and Simon P 2004 *Solid State Sci.* **6** 815
[32] Zhou S, Shi L, Zhao J, Yang H and Chen L 2007 *Solid State Commun.* **142** 634
[33] Tovar M, Alejandro G, Butera A, Caneiro A, Causa M T, Prado F and Sanchez R D 1999 *Phys. Rev.* B **60** 10199
[34] Shames A I, Rozenberg E, Markovich V, Auslender M, Yakubovsky A, Maignan A, Martin C, Raveau B and Gorodetsky G 2003 *Solid State Commun.* **126** 395
[35] Autret-Lambert C, Gervais M, Gervais F, Simon P and Raimboux N 2005 *Solid State Sci.* **7** 1035
[36] Awana V P S, Nakamura J, Karppinen M, Yamauchi H and Malik S K 2002 *J. Magn. Magn. Mater.* **250** L6